ADVANCED HEALTHCARE MATERIALS
www.advhealthmat.de

$SrCuSi_4O_{10}$/GelMA Composite Hydrogel-Mediated Vital Pulp Therapy: Integrating Antibacterial Property and Enhanced Pulp Regeneration Activity

Yu Qiu, Jun Tian, Siyi Kong, Yanping Feng, Yangyu Lu, Lefeng Su, Yanling Cai, Mengjie Li, Jiang Chang, Chen Yang,* and Xi Wei**

Vital pulp therapy (VPT) is considered a conservative treatment for preserving pulp viability in caries-induced dental pulp infections. However, bacterial contamination negatively affects dentine-pulp complex repair. The common capping materials show limited antimicrobial effects against some microorganisms. To improve the VPT efficacy, capping materials with increased antibacterial properties and enhanced odontogenic and angiogenic activities are needed. Herein, a $SrCuSi_4O_{10}$/gelatin methacrylate(SC/Gel) composite hydrogel has been proposed for infected dental pulp treatment. $SrCuSi_4O_{10}$ (SC) is a microscale bioceramic composed of assembled multilayered nanosheets that possesses good near-infrared photothermal conversion ability and multiple bioactivities due to sustained Sr^{2+}, Cu^{2+}, and SiO_3^{2-} ion release. It is shown that the SC/Gel composite hydrogel efficiently eliminates *Streptococcus mutans* and *Lactobacillus casei* and inhibits biofilm formation under photothermal heating, while the ion extract from SC promotes odontogenesis of rat dental pulp stem cells and angiogenesis of human umbilical vein endothelial cells. The as-designed therapeutic effect of SC/Gel composite hydrogel-mediated VPT has been proven in a rat dental pulp infection model and yielded improved dentine-pulp complex repair compared with the commercially used iRoot® BP Plus. This study suggests that the SC/Gel composite hydrogel is a potential pulp-capping material with improved effects on dentine–pulp complex repair in infected pulp.

1. Introduction

Dental pulp infection, which leads to pulp inflammation and necrosis, is mainly induced by cariogenic bacterial colonization and biofilm formation on dentine, defects in the dentine protecting pulp tissue, and the subsequent bacterial invasion of dental pulp.[1] The conventional endodontic therapy for the infection of mature permanent dental pulp is root canal therapy (RCT) with the removal of all pulp tissue. However, the absence of pulp vitality is disadvantageous for long-term tooth survival, so more conservative treatment strategies aimed at dental pulp vitality preservation are recommended.[2]

Vital pulp therapy (VPT), including pulp capping and pulpotomy, has been recommended for young permanent teeth with deep caries, clinically diagnosed reversible pulpitis, and even in some cases irreversible pulpitis to preserve pulp viability.[3] This therapeutic process includes the removal of infected dentine and pulp tissue, the covering of the surface of exposed pulp tissue with bioactive capping materials and the restoration of injured pulp.[4] VPT helps maintain the integrity of the

Y. Qiu, J. Tian, S. Kong, Y. Lu, Y. Cai, M. Li, X. Wei
Hospital of Stomatology
Guanghua School of Stomatology
Sun Yat-Sen University
Guangzhou, Guangdong 510055, P. R. China
E-mail: weixi@mail.sysu.edu.cn

The ORCID identification number(s) for the author(s) of this article can be found under https://doi.org/10.1002/adhm.202300546

DOI: 10.1002/adhm.202300546

Y. Qiu, J. Tian, S. Kong, Y. Lu, Y. Cai, M. Li, X. Wei
Guangdong Provincial Key Laboratory of Stomatology
Guangzhou, Guangdong 510055, P. R. China

Y. Feng, L. Su, J. Chang, C. Yang
Joint Centre of Translational Medicine
the First Affiliated Hospital of Wenzhou Medical University
Wenzhou 325000, P. R. China
E-mail: jchang@mail.sic.ac.cn; cryangchen@ucas.ac.cn

J. Chang, C. Yang
Zhejiang Engineering Research Center for Tissue Repair Materials
Wenzhou Institute
University of Chinese Academy of Sciences
Wenzhou 325000, P. R. China

J. Chang
State Key Laboratory of High Performance Ceramics and Superfine Microstructure
Shanghai Institute of Ceramics
Chinese Academy of Sciences
1295 Dingxi Road, Shanghai 200050, P. R. China

teeth and vitality of dental pulp. Furthermore, the benefits of minimally invasive care offered by VPT permit more conservative restorative care, which is also related to a reduced cost. The successful application of VPT largely depends on the complete elimination of infection in pulp because bacteria contamination negatively influence dentine-pulp complex repair.[5] Unfortunately, it is difficult to determine the extent of pulp infection because the clinical symptoms and pathological characteristics are sometimes inconsistent.[6] Moreover, bacterial contamination in serious caries cases is nearly impossible to completely remove through infection removal operations, and biofilm formation further increases the difficulty of eliminating bacterial contamination.[7] The currently applicable biologically active capping materials, such as calcium hydroxide and calcium silicate-based cements, have been proven to exhibit antibacterial properties, promote odontogenic differentiation of dental pulp cells, and induce the formation of a reparative hard-tissue bridge. However, several studies have found that these capping materials exerted limited antimicrobial effects against some microorganisms,[8] which may lead to the failure of VPT. Therefore, novel capping materials with improved antibacterial and antibiofilm effects as well as the ability to stimulate hard-tissue barrier production are needed.

To rapidly kill bacteria and inhibit long-term bacterial growth, a variety of approaches have been developed, such as the application of antibacterial metal ions and high temperature.[9] Copper (Cu), an element with significant antibacterial activity, has been widely incorporated into biomaterials to kill bacteria. However, its antibacterial effect is dependent on Cu being present in a sufficiently high concentration and requires a long time, which decreases antibacterial efficiency.[10] Another disadvantage of Cu is that a high concentration of Cu ions is possibly toxic to normal tissues.[11] In recent years, photothermal therapy (PTT), which is based on local high temperature produced by photothermal agents under near infrared (NIR) irradiation, has emerged as a promising effective antibacterial method. A sufficiently high temperature has been suggested to cause irreversible cell damage by denaturing proteins or enzymes, blocking metabolic signals, breaking down the cell membrane of microbes, and leading to the leakage of cellular content.[12] In contrast to antibiotic or metal ions, PTT exhibits a rapid antibacterial effect on various types of bacteria and reduces bacterial resistance.[9b,13] In previous studies, the application of photothermal agents with 808 nm NIR irradiation for 15 min has been found to exert an excellent antimicrobial effect in vitro and in vivo.[14] Nevertheless, bacteria may regrow once the temperature decreases, and long-term high temperatures can also damage normal cells.[15] Recently, the combination of Cu and polydopamine induced PTT has been suggested to have synergistic effects, with an increased long-term antibacterial effect and a lower operating temperature of 50 °C, decreasing thermal damage to normal tissue.[16] However, it is unknown whether this treatment has antibacterial effects on caries-induced infected dental pulp.

On the other hand, to achieve successful reparative dentine formation and dental pulp regeneration, inorganic materials have been widely applied in VPT owing to the sustained release of bioactive ions. Silicon (Si) has been shown to have positive effects on the odontogenic differentiation of dental pulp stem cells (DPSCs) and vascularization of endothelial cells (ECs).[17] Silicate biomaterials have been demonstrated to improve hard tissue formation as well as blood vessel regeneration, which contributes to the immune response and antibacterial effect as well as the pulp nutrient supply for cell viability and pulp tissue regeneration.[18] Silicate can combine with metal cations, such as Cu ions and strontium (Sr) ions. The addition of these bioactive metal ions improves the odontogenesis and angiogenesis effects of silicate materials.[19] Therefore, it is assumed that synthetic materials, including Si, Cu, and Sr, may exhibit excellent bioactivity for repairing the dentine-pulp complex.

Based on the above considerations, we hypothesized that treatment with $SrCuSi_4O_{10}$ (SC) combined with high temperature may exert antibacterial and antibiofilm effects and facilitate dentine formation and vascularization. The photothermal property of SC was demonstrated and applied to eliminate bone tumors in a previous study.[20] However, it is unclear whether treatment with SC combined with heat has antibacterial effects. Although the ability of SC to promote vascularized bone regeneration has been proven,[21] its therapeutic effects on dental pulp regeneration remain unknown. Therefore, we hypothesized that the application of SC as the pulp-capping material together with PTT can eliminate bacteria and promote the success of VPT for infected dental pulp due to the enhanced odontogenesis and angiogenesis.

To apply SC to infected pulp, we chose gelatin methacryloyl (GelMA) hydrogel as the carrier material to load SC microparticles due to its great biocompatibility and easy crosslinking by UV light,[22] which can directly contact pulp tissue and exactly cover exposed dental pulp to form a barrier protecting the pulp tissue (**Figure 1**). Therefore, we prepared a $SrCuSi_4O_{10}$/GelMA (SC/Gel) composite hydrogel with detailed characterizations and evaluated its antibacterial and antibiofilm activities under NIR light using *Streptococcus mutans* (*S. mutans*) and *Lactobacillus casei* (*L. casei*). Then, we established a rat dental pulp infection model induced by deep caries-related bacteria and investigated the therapeutic effect using composite hydrogel combined with PTT. Moreover, the ability and potential mechanisms of SC to induce odontogenesis and angiogenesis were evaluated using rat dental pulp stem cells (rDPSCs) and human umbilical vein endothelial cells (HUVECs). This study provides a new avenue for developing capping biomaterials to be applied to infected mature permanent dental pulp and to improve the outcome of VPT.

2. Results

2.1. Synthesis and Characterization of $SrCuSi_4O_{10}$ Microparticles

$SrCuSi_4O_{10}$ microparticles were synthesized through a hydrothermal method. The low-magnification scanning electron microscope (SEM) image of the synthesized SC microparticles revealed that they were pancake-like in shape and uniform with a diameter of ≈12 µm and thickness of ≈4 µm (**Figure 2**a). Higher magnification SEM images of the SC microparticles further showed that they were composed of multilayered nanosheets assembled in an ordered way (Figure 2b). Energy-dispersive X-ray spectroscopy (EDS) elemental mapping of the SC microparticles demonstrated the homogeneous distribution of Sr, Cu, Si, and O (Figure 2c), while the X-ray diffraction (XRD) patterns of the SC microparticles confirmed their structure and phase purity according to the standard ICSD Card (No. 81–1239, Figure 2d). More-

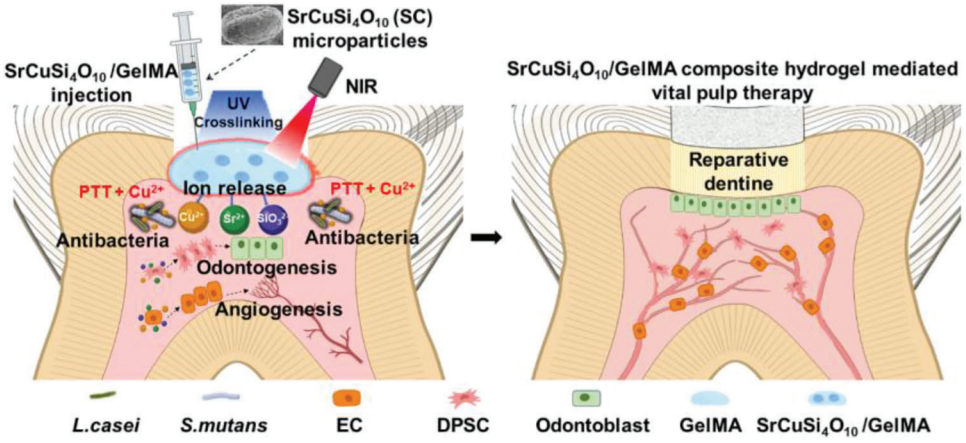

Figure 1. Schematic illustration of the application of SC/Gel composite hydrogel and NIR irradiation for infected dental pulp treatment, through releasing Sr^{2+}, Cu^{2+}, and SiO_3^{2-} ion in response to the promoted antibacterial effect, angiogenesis, and odontogenesis.

over, Fourier transform infrared (FTIR) spectroscopy (Figure 2e) confirmed the successful synthesis of SC microparticles by the presence of absorption bands of Si–O–Si (472 cm^{-1}),[23] Cu–O (519, 586, and 659 cm^{-1}),[24] Sr–O (855 cm^{-1}),[25] and Si–O (1048 and 1159 cm^{-1}).[26] The inductively coupled plasma mass spectrometer (ICP–MS) results showed ion concentrations of Si, Cu, and Sr in the SC extracts (Figure S1a, Supporting Information). Finally, the UV–vis-NIR absorption spectrum (Figure 2f) revealed that the SC microparticles had two absorption peaks at 628 and 798 nm, indicating that the SC microparticles could be excited by NIR laser light (e.g., 808 nm laser) to generate a photothermal effect.

2.2. Preparation and Characterization of the $SrCuSi_4O_{10}$/GelMA Composite Hydrogel

The SC/Gel composite hydrogel was prepared by dispersing the SC microparticles in GelMA solution. As shown in Figure 2g, the mixture transformed from solution into a gel after UV crosslinking (Figure 2g). The optical images of the SC/Gel composite hydrogels with various concentrations of SC microparticles (0.5, 1, and 2 wt.%) are presented as the 0.5-SC/Gel, 1-SC/Gel, and 2-SC/Gel groups (Figure 2h). The color of the composite hydrogels turned dark blue with an increase in the amount of incorporated SC microparticles. SEM images further revealed that the SC microparticles were homogeneously encapsulated in the hydrogel network without distinctly altering the porous structures of the hydrogel (Figure 2h). The ICP–MS results showed the ion concentrations of Cu in the extracts of the SC/Gel composite hydrogels (Figure S1b, Supporting Information).

The photothermal performance of different hydrogels was then investigated under 808 nm laser irradiation at a power density of 1 W cm^{-2} for 5 min. Almost no temperature elevation was observed in the pure GelMA group after laser irradiation. However, the temperature of the composite scaffolds dramatically increased after irradiation with 808 nm light, and an obvious concentration-dependent temperature increase was observed. The maximum temperature elevations of the 0.5-SC/Gel, 1-SC/Gel, and 2-SC/Gel groups were ≈20.3, 29.4, and 37.3 °C, respectively (Figure 2i). In addition to the content of embedded SC microparticles, the photothermal performance of the composite hydrogel was also dependent on the laser power density (Figure 2j). The infrared thermal images showed the temperature elevation of 0.5-SC/Gel composite hydrogels under 808 nm laser (1.5 W cm^{-2}) at different times (Figure S2, Supporting Information). Moreover, no particular temperature change was observed after 5 repetitive laser on/off cycles, implying the photothermal stability of the SC/Gel composite hydrogel (Figure 2k).

2.3. Antibacterial Activity of the $SrCuSi_4O_{10}$/GelMA Hydrogel

S. mutans and *L. casei* were selected to evaluate the antibacterial effect of the SC/Gel hydrogel and NIR irradiation. Bacteria treated with iRoot BP Plus (BP), GelMA hydrogel, GelMA hydrogel together with NIR irradiation, SC/Gel hydrogel or SC/Gel hydrogel together with NIR irradiation were defined as the BP, Gel, Gel+NIR, SC/Gel, and SC/Gel+NIR groups. To explore the rapid bacterial killing effect, the pathogens were collected immediately after treatment with the hydrogels combined with or without 15 min of NIR irradiation, and then the colonies were counted after separation on agar plates. As a control material, BP did not significantly change the number of colonies. The bacterial colony number of the Gel group was slightly greater than that of the control group, but the difference was not statistically significant. The Gel+NIR group exhibited a bacterial colony number similar to that of the Gel group. Compared to the control, Gel and Gel+NIR groups, the SC/Gel group had a markedly reduced colony number of both *S. mutans* and *L. casei*. Moreover, the SC/Gel +NIR group showed the lowest bacterial colony number of all groups for both bacteria (**Figure 3**a,e). The *S. mutans* survival percentages of the BP, Gel and Gel+NIR, SC/Gel, and SC/Gel+NIR groups were 124.13%, 131.56%, 103.96%, 1.32%, and 0%, respectively (Figure 3b). The *L. casei* survival percentages of the BP, Gel, and Gel+NIR, SC/Gel and SC/Gel+NIR groups were 68.56%, 125.05%, 119.82%, 29.52%, and 0%, respectively (Figure 3f). These results revealed that the SC/Gel hydrogel combined with NIR irradiation had the lowest bacterial survival rate.

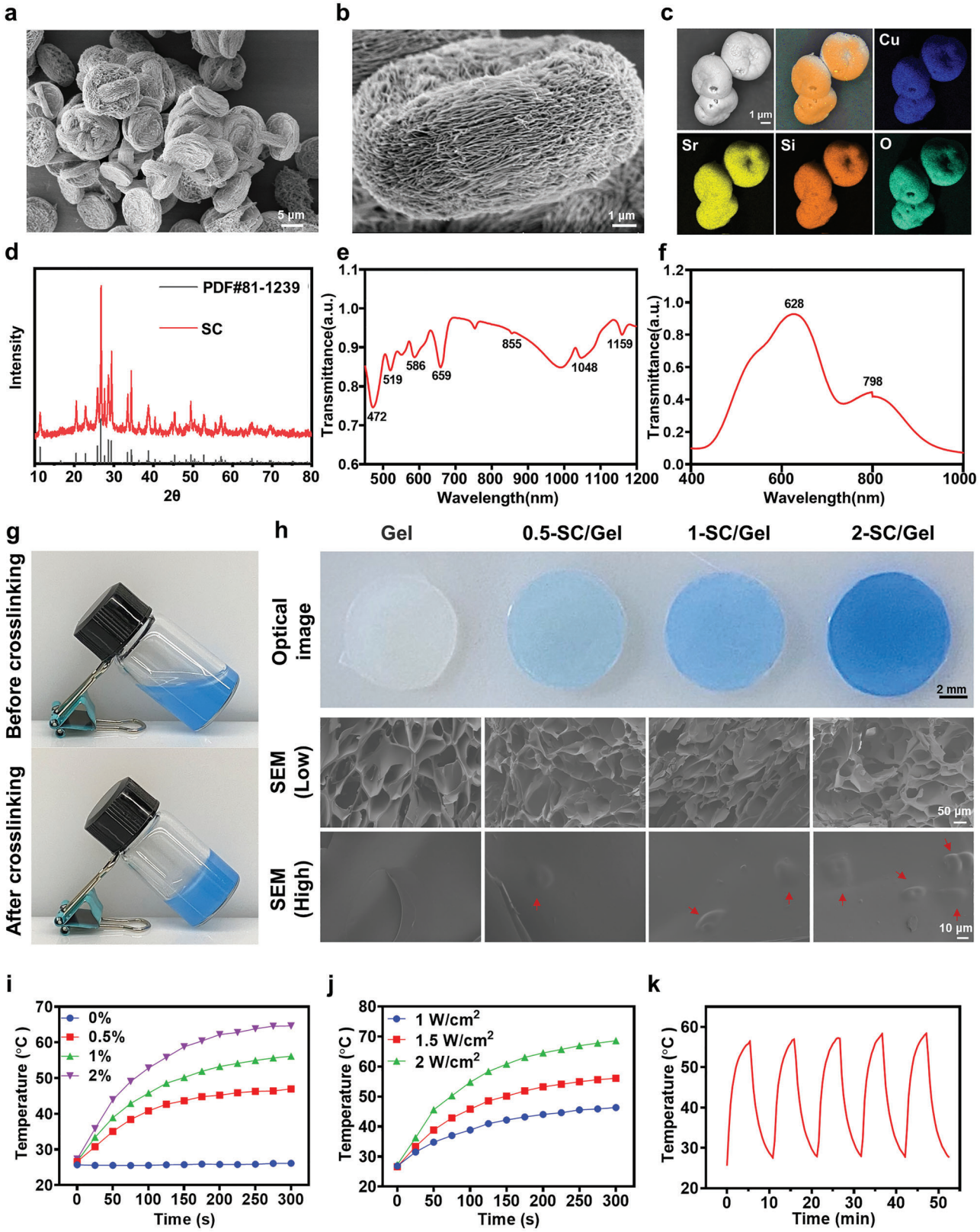

Figure 2. Characterization of SC microparticles and SC/Gel composite hydrogels. a,b) SEM images of SC microparticles. c) Images of the EDS elemental mapping of Sr, Cu, Si, and O in SC microparticles. d) XRD patterns of SC microparticles. e) FTIR spectrum of SC microparticles. f) UV–vis-NIR absorption spectrum of SC microparticles. g) SC/Gel mixture transformed from solution into a gel after UV crosslinking. h) Pictures and SEM images of

For the bacterial growth inhibition study, a spot assay and the optical density (OD) method were used to evaluate the effect of the SC/Gel composite hydrogel and NIR on the proliferation of *S. mutans* and *L. casei*. The spot assay pictures showed that the bacterial colonies of the control, BP, Gel and Gel+NIR groups had similar sizes, and those of the SC/Gel and SC/Gel+NIR groups were significantly smaller than those of the other groups (Figure 3c,g). The OD600 results indicated that the SC/Gel and SC/Gel+NIR groups had decreased bacterial growth, while the BP group did not. Compared to the SC/Gel group, the SC/Gel+NIR group showed more significant inhibition activity. However, no obvious difference was observed between the Gel and Gel+NIR groups (Figure 3d,h).

2.4. Biofilm Formation Inhibition of the $SrCuSi_4O_{10}$/GelMA Hydrogel

Biofilms formed by the coculture of *S. mutans* and *L. casei* were selected to investigate the inhibitory effects of the SC/Gel hydrogel and NIR irradiation on biofilm formation. The crystal violet staining results indicated that the control, BP, Gel, and Gel+NIR groups had similar biofilm biomasses. Moreover, the SC/Gel hydrogel significantly inhibited biofilm formation. After treatment with NIR irradiation, the SC/Gel hydrogel exerted the strongest inhibitory effect on biofilm formation (**Figure 4**a). The live/dead staining images of the remaining biofilms also indicated a similar trend. The live and dead bacteria of the biofilms were separately indicated by the green and red fluorescence. The biofilms of the control, BP, Gel, and Gel+NIR groups had analogous densities and extremely complete green fluorescence. For the SC/Gel group, a decreased biofilm biomass and some yellow fluorescence, which was overlaid with green and red fluorescence, were observed. In comparison, with NIR irradiation, a reduced biofilm density and greatly increased yellow fluorescence were observed for the SC/Gel group (Figure 4b). All of the above results suggested that the SC/Gel hydrogel inhibited *S. mutans* and *L. casei* biofilm formation and that the addition of NIR irradiation further enhanced the inhibitory effect.

2.5. In Vivo Infected Pulp Tissue Regeneration and Dentine Repair

The bacteria-induced rat dental pulp infection model was established using *S. mutans* and *L. casei*. Procedure for pulp infection induction and treatment with the SC/Gel hydrogel and NIR irradiation was illustrated (**Figure 5**a) and recorded by pictures (Figure S3, Supporting Information). At week 6 after direct pulp capping using the SC/Gel hydrogel combined with 15 min NIR irradiation, microcomputed tomography (micro-CT) analysis of the treated teeth was employed to examine reparative dentine bridge formation at the site of the defect (Figure 5b). The images suggested intact dentine bridges in the blank group (sound teeth). In the control group (bacterial infected teeth) and the SC/Gel group, a dentine bridge was barely formed, while an apparent thick mineralization bridge was observed above the pulp chamber in the SC/Gel+NIR group. The quantitative analysis of newly formed tertiary dentine in pulp chambers (marked by the red broken lines) suggested significantly less reparative dentine in the control and SC/Gel groups than in the blank group. In contrast, in the SC/Gel+NIR group, the volume of the mineralization bridge markedly increased compared to that in the control group and the SC/Gel group (Figure 5c).

A histological analysis was performed to evaluate the grades of inflammation and mineralization in pulp tissue (**Table 1**) and observe reparative dentine formation and vascularization (Figure 5d). In the blank group, complete and homogenous reparative dentine was formed, and the pulp tissue was basically normal with an organized odontoblast-like layer and collage structure and a mild inflammatory response. Blood vessels were observed without obvious expansion or hyperplasia. In the control group, instead of normal pulp tissue and odontoblasts in the pulp chamber, there was incomplete disordered calcified tissue entrapping necrotic tissue, and severe inflammatory infiltrate was detected around the calcified tissue. Blood vessel expansion and hyperplasia and tissue edema were observed in the residual pulp tissue. In the SC/Gel group, necrotic tissue and inflammatory cells under the cavity and blood vessel expansion were also observed, although the extent was slightly lower than that in the control group. No complete dental bridge was detected. In the SC/Gel+NIR group, extensive and complete newly generated hard tissue with a dentinal tubule structure was observed in the pulp-material interface, and odontoblast-like cells were arranged beneath the reparative dentine. A mild inflammatory response was observed for the pulp tissue near the injured site. No evident blood vessel expansion or structural damage was found in the pulp tissue. The measurement of tertiary dentine thicknesses confirmed the significant negative effect of bacterial infection on dentine formation and the positive effect of the SC/Gel hydrogel combined with NIR irradiation and the ineffectiveness of the SC/Gel hydrogel alone on dentine formation in infected pulp (Figure 5f).

In addition, dentine formation measured by the expression of dentine sialophosphoprotein (DSPP) and angiogenesis measured by the expression of platelet endothelial cell adhesion molecule-1 (CD31) were further investigated by immunofluorescence (IF) (Figure 5e,g,h). The staining images showed that bacterial infection decreased the expression of DSPP and CD31, that the SC/Gel hydrogel did not reverse this trend, and that the SC/Gel hydrogel combined with NIR irradiation did have the opposite effect. Moreover, histological images of the heart, liver, spleen, lung, and kidney revealed that the SC/Gel hydrogel processed no toxicity to major organs (Figure S4, Supporting Information). All these results indicated that the SC/Gel hydrogel combined with NIR irradiation can promote the repair of the dentine-pulp complex of infected pulp.

SC/Gel composite hydrogels with various concentrations of SC microparticles (0.5, 1, and 2 wt.%). i) Photothermal-heating curves of SC/Gel composite hydrogels with various concentrations of SC microparticles (0.5, 1, and 2 wt.%) under irradiation with an 808 nm laser at a power density of 1.0 W cm^{-2} for 300 s. j) Photothermal-heating curves of the 0.5-SC/Gel composite hydrogel under irradiation with an 808 nm laser at different power densities (1.0, 1.5, and 2 W cm^{-2}) for 300 s. k) Heating curves of the SC/Gel composite hydrogel for five laser on/off cycles under irradiation with an 808 nm NIR laser (1.5 W cm^{-2}). The data are expressed as the means ($n = 3$).

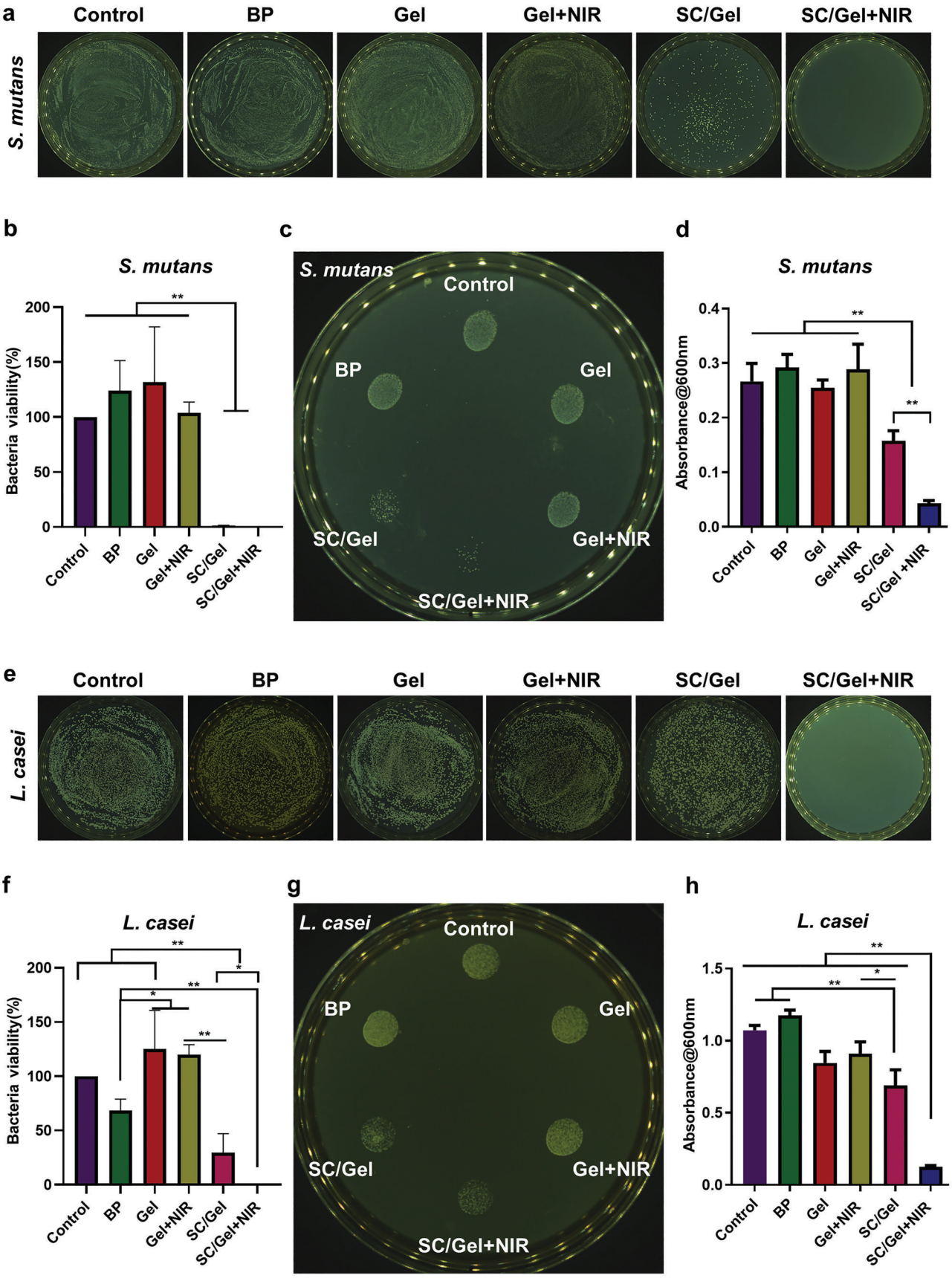

Table 1. Grading of the histological sections of the pulps in each group.

		Pulp inflammation grade					Pulp mineralization grade			
Group	n	0	1	2	3	Median	0	1	2	Median
Blank	5	2	3	-	-	$1^{A)}$	-	5	-	$1^{a),b)}$
Control	6	-	-	2	4	$3^{B)}$	4	2	-	$0^{a)}$
SC/Gel	4	-	-	2	2	$2.5^{B),C)}$	1	3	-	$1^{a),b)}$
SC/Gel+NIR	5	-	5	-	-	$1^{A),C)}$	-	2	3	$2^{b)}$

$^{A,B,C)}$ Different capital letters indicate statistical differences for the Kruskal–Wallis H test and following Dunn's post hoc test. Same capital letters do not indicate statistical differences. For the grades of pulp inflammation, significant differences ($p < 0.05$) were found between the control and SC/Gel groups and the blank group, and between the control group and the SC/Gel+NIR group. $^{a,b)}$ Different lowercase letters indicate statistical differences for the Kruskal–Wallis H test and following Dunn's post hoc test. Same lowercase letters do not indicate statistical differences. For the grades of pulp mineralization, a significant difference ($p < 0.05$) was found between the control group and the SC/Gel+NIR group.

2.6. $SrCuSi_4O_{10}$ Enhanced the Viability and Migration of rDPSCs and HUVECs

rDPSCs were characterized by flow cytometry and adipogenic and osteogenic induction. The results showed the positive expression of mesenchymal stem cell surface markers (CD29, CD44, and CD90) and the negative expression of the hematopoietic markers (CD34 and CD45) (Figure S5a, Supporting Information). Mineralized nodules and lipid droplet formation demonstrated the multipotent differentiation capacity of cells (Figure S5b,c, Supporting Information). These results suggested that cultured rDPSCs possessed the mesenchymal phenotype of mesenchymal stem cells.

To investigate the effects of SC on the proliferation of rDPSCs and HUVECs, we cultured cells in various dilutions (1/2, 1/4, 1/8, 1/16, 1/32, 1/64, 1/128, and 1/256) of SC microparticle extracts for 1, 3, and 5 days. Cell counting kit (CCK) – 8 assays showed that SC at low concentrations (1/256) did not influence cell viability. Medium concentrations (1/16 and 1/32) of SC increased the viability of both rDPSCs and HUVECs on days 3 and 5. However, rDPSCs and HUVECs treated with SC at high concentrations (1/2 and 1/4) had significantly decreased viabilities after culturing for 1, 3, and 5 days (**Figure 6**a,b). The live/dead cell staining images confirmed the cell compatibility of SC extracts at 1/16 and 1/32 dilutions (Figure 6c). Overall, 1/16 and 1/32 were favorable dilution ratios for cell proliferation.

The effects of SC on the migration of rDPSCs and HUVECs were examined by Transwell assays (Figure 6d). In the 1/16 group, the number of migrated HUVECs was significantly increased, but that of rDPSCs was not. Compared with those in the control group, more migrated rDPSCs and HUVECs were observed in the 1/32 group. Taken together, these results suggested that SC extract at a 1/32 dilution ratio significantly promoted both the viability and migration of rDPSCs and HUVECs. Thus, the 1/32 dilution was chosen as the optimal concentration for the following experiments.

2.7. $SrCuSi_4O_{10}$ Induced the Odontogenesis of rDPSCs

Cells precultured with normal culture medium or the extract of SC microparticles or BP were defined as the OM, SC, and BP groups. Alizarin Red S staining analysis demonstrated that after 21 days of culturing under osteogenic conditions, mineralized nodules were obviously deposited in the OM group. In both the BP and SC groups, developed mineralization was observed compared to the OM group, and the SC group showed slightly more mineralization. The qualitative analysis of calcium deposits showed the same trend (**Figure 7**a). Moreover, the qPCR results at day 7 indicated that the OM group promoted the expression of odontogenic genes, including *DSPP*, dentine matrix acid phosphoprotein-1 (*DMP1*), and bone sialoprotein (*BSP*), and the SC group enhanced the expression of *DMP1* and *BSP* similarly to the BP group and promoted *DSPP* expression compared to the BP group (Figure 7b).

2.8. $SrCuSi_4O_{10}$ Promoted the Angiogenesis of HUVECs

To evaluate the in vitro angiogenic abilities of SC, a tube formation assay was carried out. The tubule formation images showed that HUVECs cultured with SC microparticle extract in the SC group for 8 h exhibited more tube networks, short lines, and mesh-like circle formation than those in the control group and BP group. The quantitative analysis verified that the SC group had a significantly increased total length and number of nodes of newly formed tubes, with a weak enhancement compared to the BP group (Figure 7c). In addition, the expression of angiogenesis-related genes such as vascular endothelial growth factor (*VEGF*), kinase-domain receptor (*KDR*), *CD31*,

Figure 3. Antibacterial ability of the SC/Gel hydrogel and NIR laser (15 min, 1.5 W cm^{-2}). a,b) The SC/Gel hydrogel both with or without NIR irradiation rapidly reduced the colony numbers of *S. mutans* compared to the other treatments, and the negative effect on bacterial viability was revealed by quantitative analysis after counting CFU of serially diluted (1:10) dilution samples. c,d) Images of *S. mutans* cultured with hydrogels for 24 h showed inhibited bacterial growth in the SC/Gel and SC/Gel+NIR groups, which was demonstrated by the OD600 results. Compared to the SC/Gel hydrogel, the SC/Gel hydrogel combined with NIR irradiation showed a more significant antibacterial effect. e,f) The SC/Gel hydrogel rapidly reduced the colony number of *L. casei* compared to the other groups, and NIR irradiation further improved this effect. The quantification data of bacterial colonies indicated these significant differences. g,h) The growth of *L. casei* cultured with the SC/Gel hydrogel for 24 h was inhibited. The OD600 results showed that the SC/Gel hydrogel decreased bacterial proliferation, and the SC/Gel hydrogel combined with NIR irradiation resulted in the lowest amount of bacterial growth. The data are expressed as the means ± SDs ($n = 3$), p-values were calculated by one-way analysis of variance (ANOVA) with Tukey's multiple comparison: not significant, $p > 0.05$;*$p < 0.05$; **$p < 0.01$.

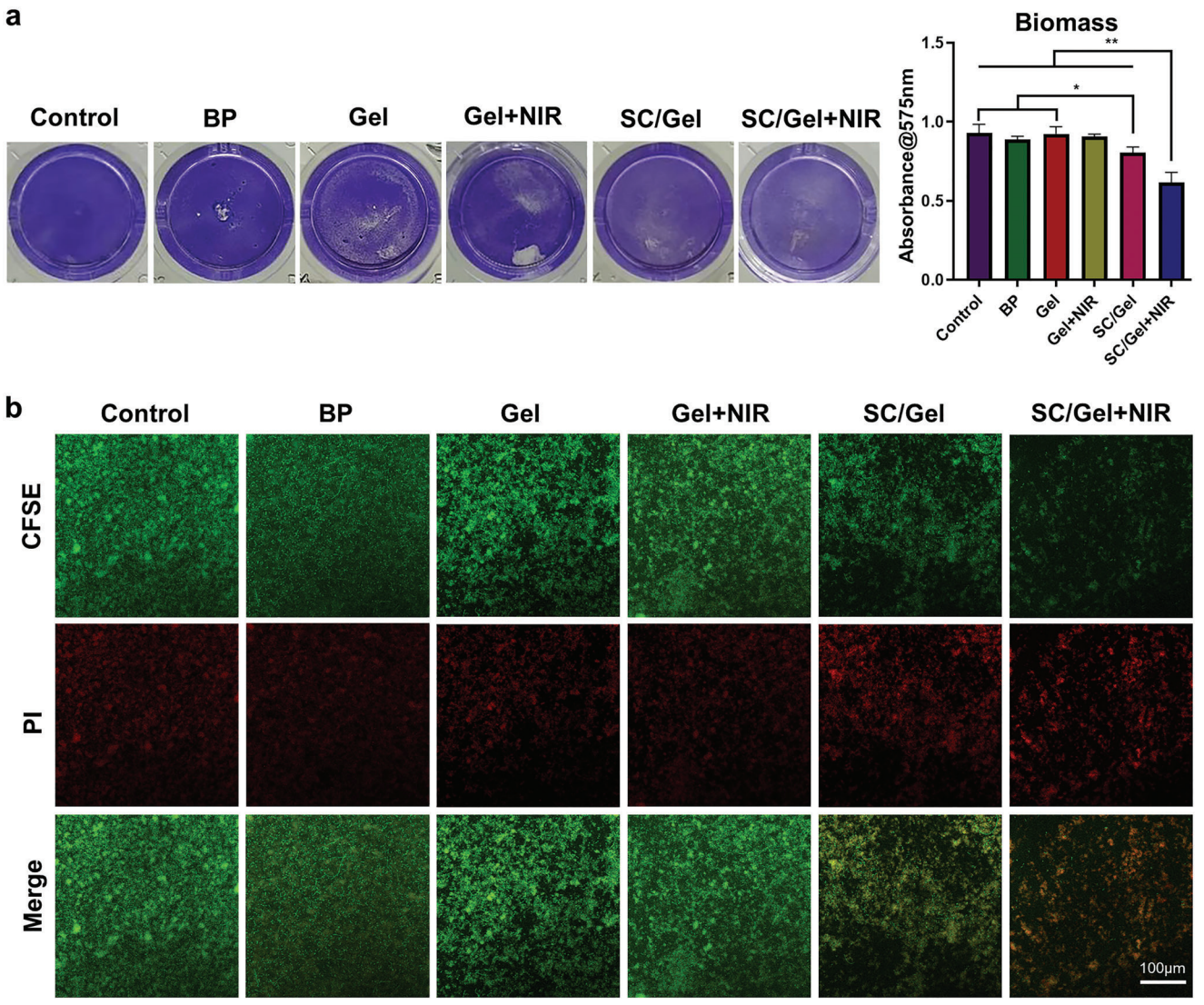

Figure 4. Inhibition effect of the SC/Gel hydrogel and NIR laser (15 min, 1.5 W cm^{-2}) on biofilm formation. a) The crystal violet staining and OD575 results showed that the SC/Gel group exhibited inhibited biofilm formation compared to the control, BP, Gel, and Gel+NIR groups. Moreover, after treatment with NIR irradiation, the SC/Gel hydrogel exerted the strongest inhibitory effect on biofilm formation. b) The live/dead staining images of the remaining biofilms showed biofilms with decreased thicknesses consisting of less live bacteria and more dead bacteria in the SC/Gel group, and the addition of NIR irradiation further enhanced the antibiofilm effect in the SC/Gel group. The data are expressed as the means ± SDs ($n = 3$), p-values were calculated by one-way ANOVA with Tukey's multiple comparison: not significant, $p > 0.05$; $^{*}p < 0.05$; $^{**}p < 0.01$.

stromal cell-derived factor-1 (*SDF1*), and hypoxia-inducible factor 1-α (*HIF1*α) was higher in the SC group than in the control group and BP group (Figure 7d). These findings suggested that SC promoted the expression of angiogenesis-related genes and improved the angiogenesis of HUVECs.

3. Discussion

For VPT, calcium silicate-based materials, such as mineral trioxide aggregate (MTA) and BP, have been indicated to be effective pulp-capping materials on the basis of the absolute elimination of infection.[27] However, the inadequate antibacterial properties of these materials restrict their therapeutic effect on infected exposed dental pulp.[28] In this study, we fabricated a $SrCuSi_4O_{10}$/GelMA composite hydrogel and proved that the application of the composite hydrogel combined with PTT may be a useful strategy of direct pulp-capping for infected mature permanent dental pulp. Our results demonstrated the favorable physical properties, photothermal performance, ion release properties, and biocompatibility of the $SrCuSi_4O_{10}$/GelMA composite hydrogel. Furthermore, the composite hydrogel obviously promoted odontogenesis and angiogenesis and inhibited bacterial growth and biofilm formation.

In the present study, to establish an infected rat molar model, we added *S. mutans* and *L. casei* onto exposed dental pulp, which is quite different from a previous study in which *Enterococcus faecalis* (*E. faecalis*) was chosen to induce pulpal infection.[29] Since *Streptococcus* and *Lactobacillus* are pathogens commonly found in

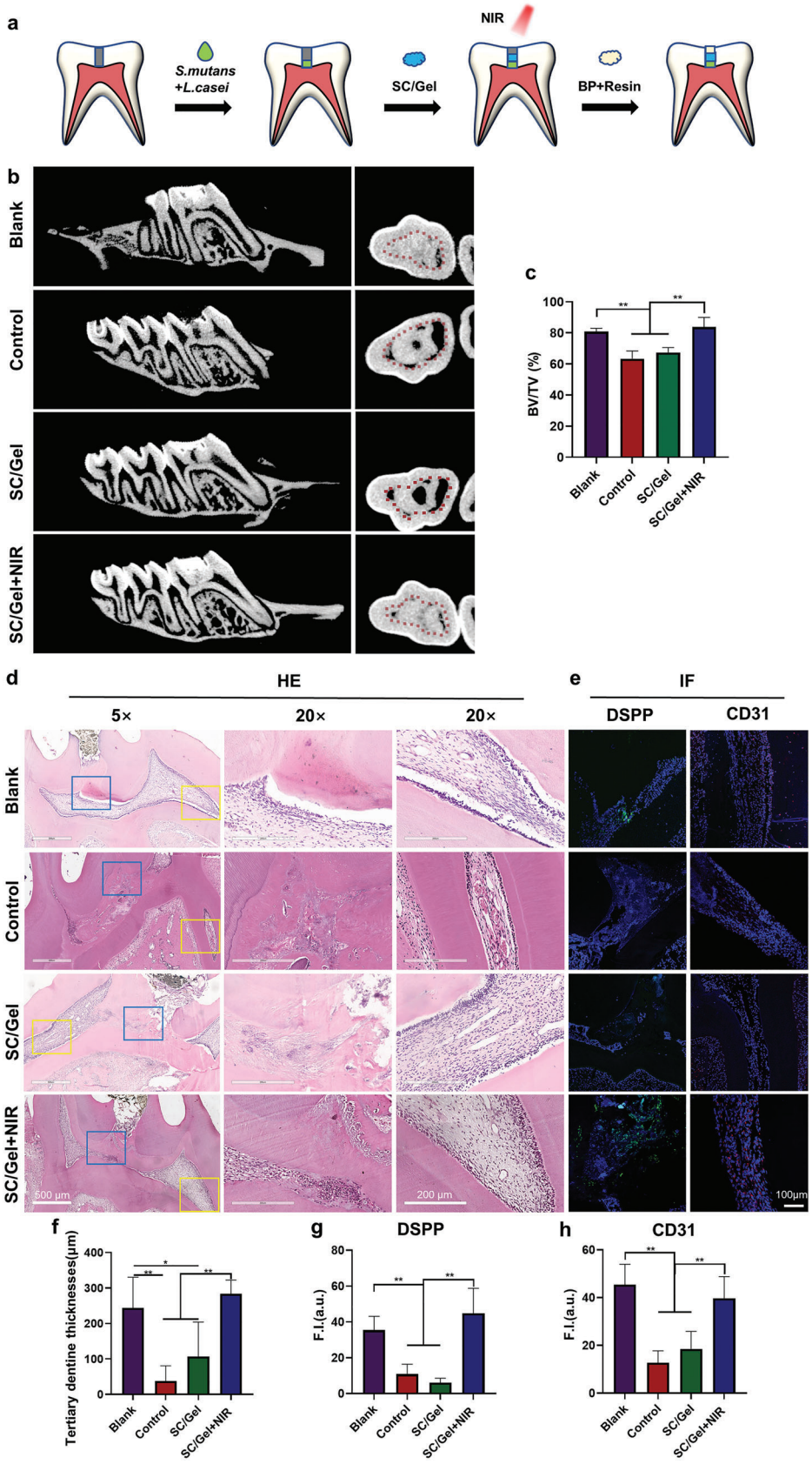

Figure 5. Evaluation of dentine-pulp complex repair after using the SC/Gel hydrogel combined with NIR irradiation in the pulp capping of infected pulp in vivo. a) Procedure for pulp infection induction, treatment with the SC/Gel hydrogel and NIR irradiation and restoration with dental composite resin

the deep caries cavities or carious exposed dental pulp of human teeth,[30] whereas *E. faecalis* has been implicated in persistent endodontic treatment failure,[31] we selected *S. mutans* and *L. casei*, rather than *E. faecalis*, to simulate early carious pulp infection. In our study, H&E staining, immunofluorescence staining, and micro-CT analysis confirmed the severe inflammation and necrosis, vascular structural disruption, and incomplete disordered calcification of the dental pulp infected with *S. mutans* and *L. casei*, indicating the ability of *S. mutans* and *L. casei* to induce pulp infection and irreversible inflammation.

BP is a pre-mixed bioceramic putty material with similar cytotoxicity, antibacterial efficacy, and ability to promote complete calcified bridge formation in comparison with the classic pulp capping material MTA.[8b,32] Interestingly, our results showed the weak antibacterial function of BP against *S. mutans* and *L. casei* in vitro. Moreover, BP could not induce adequate pulp repair in *S. mutans*- and *L. casei*-infected pulp. The alkaline environment resulting from the hydration reaction of BP contributes to the antibacterial effect of BP.[8b] However, the hydration reaction only appears in the initial phase of contact of BP with water and occurs quickly, contributing to the minor effect of BP on eliminating *S. mutans* and *L. casei*. In published studies, the antibacterial activities of BP remain controversial, which may be because of the use of different bacterial strains and methodologies.[30b] In contrast, after treatment with the $SrCuSi_4O_{10}$/GelMA hydrogel and NIR irradiation, the dental pulp exhibited satisfactory reparative performance. Similarly, the in vitro experiment results indicated the photothermal properties of the $SrCuSi_4O_{10}$/GelMA hydrogel, in accordance with previous studies, and the absolute bacterial-killing capability of the $SrCuSi_4O_{10}$/GelMA hydrogel combined with NIR irradiation was much stronger than that of the other treatments, including the BP treatment. For $SrCuSi_4O_{10}$/GelMA, 808 nm NIR light triggered photothermal heating for 15 min could provide effective antibacterial activities without causing evident damage to normal tissue in this study, and the same finding was also found with other photothermal agents in previous studies.[14,33] Without NIR irradiation, the $SrCuSi_4O_{10}$/GelMA composite hydrogel also exhibited good rapid-killing activity and growth inhibition effects on both bacteria, especially on *S. mutans*, possibly owing to the antibacterial capability of Cu ions. Cu ions are a dose-dependent antibacterial agent that can damage the cell membrane of bacteria and degrade DNA.[34] To minimize the cytotoxicity of Cu ions, 0.5 wt.% SC/Gel was applied because the released Cu ion concentration (0.034 мм) was detected to be within the reported ion concentration range of 10^{-5}–10^{-4} м, which resulted in an antibacterial rate higher than 90% and no cytotoxicity to mammalian cells.[10a] However, the separately applied $SrCuSi_4O_{10}$/GelMA composite hydrogel did not exert favorable therapeutic effects on infected dental pulp, indicating that its antimicrobial effects were not sufficient to restore the balance between inflammation and regeneration. After NIR irradiation, the $SrCuSi_4O_{10}$/GelMA composite hydrogel showed enhanced rapid and long-term antibacterial effects, suggesting the synergistic sterilization performance of the $SrCuSi_4O_{10}$/GelMA hydrogel and PTT. These results are in accordance with the previously confirmed "hot Cu ion" effect, which refers to the synergistic antibacterial effect induced by Cu ions at biocompatible low concentrations and under high temperatures. In addition, Sr has antibacterial abilities, but whether a "hot Sr ion" effect exists is unknown.

Bacterial biofilms usually form on the dentine surrounding exposed pulp tissue and increase the difficulty of eliminating bacterial contamination.[7] Thus, the antibiofilm properties of pulp capping material are imperative for dental pulp regeneration. As expected, our results did not show the ability of BP to inhibit biofilm formation by *S. mutans* and *L. casei* coculture. In comparison, the $SrCuSi_4O_{10}$/GelMA hydrogel slightly reduced the residual biofilm, and the concomitant application of the $SrCuSi_4O_{10}$/GelMA composite hydrogel and PTT had the best efficacy of inhibiting biofilm formation, in agreement with the antibacterial assay results. Cu was demonstrated to inhibit optimal biofilm development, and high temperature (50 °C) promoted the antibiofilm effect.[35] Our results suggested the synergistic ability of $SrCuSi_4O_{10}$/GelMA hydrogel and PTT to inhibit biofilm formation.

Although the addition of Cu ions lowered the bacteria-killing temperature, a temperature of 50 °C may still be harmful to the regeneration of dental pulp, according to published literature suggesting that high temperature (42 °C) reduced the number and viability of human dental pulp cells.[36] Therefore, in addition to antibacterial ability, high biological activity is also required for pulp-capping materials. We applied Sr and Si in the present material to enhance the proliferation, migration, and odontogenesis of rDPSCs and promote reparative dentine formation in rats. Sr and Si may contribute to the induction of BSP, DMP1, and DSPP expression.[17a,37] DMP1 can promote the odontoblastic differentiation of DPSCs and induce the formation of reparative dentine.[38] BSP is a signaling molecule involved in morphogenesis and odontoblast differentiation.[39] During dentine development after the formation of the predentine matrix, DSPP is known as a marker of the odontogenic differentiation of DPSCs and plays an important role in this process.[40] Our results revealed that $SrCuSi_4O_{10}$ showed an ability to promote the odontogenic differentiation of rDPSCs that was slightly better than that of BP, as indicated by the Alizarin Red S staining results and the upregulated *BSP*, *DMP1*, and *DSPP* expression. From the animal experimental data, we noticed that tertiary dentine formed not only at the injured site but also under surrounding residual dentine in the SC/Gel+NIR group. It was supposed that the high temperature caused a degree of cellular injury and led to a

(Resin). b) Micro-CT images clearly showing intact dentine bridges beneath the pulp-capping material in the blank and SC/Gel+NIR groups and no apparent dentine bridges in the control and SC/Gel groups. c) Analysis of the ratio of bone volume to tissue volume suggesting the development of mineralization bridge formation in the blank and SC/Gel+NIR groups compared to that in the control and SC/Gel groups. d,f) Hematoxylin and eosin (H&E) staining images showing excellent reparative dentine formation (marked by blue borders) and vascularization (marked by yellow borders) in the blank and SC/Gel+NIR groups compared with the control and SC/Gel groups. Measurement of the tertiary dentine thicknesses confirmed significant differences. e,g,h) Enhanced expression of DSPP and CD31 in the blank and SC/Gel+NIR groups compared to that in the control and SC/Gel groups revealed by immunofluorescence. Fluorescence intensity analysis indicated the same trend. The data are expressed as the means ± SDs ($n = 6$), p-values were calculated by one-way ANOVA with Tukey's multiple comparison: not significant, $p > 0.05$; $^{*}p < 0.05$; $^{**}p < 0.01$.

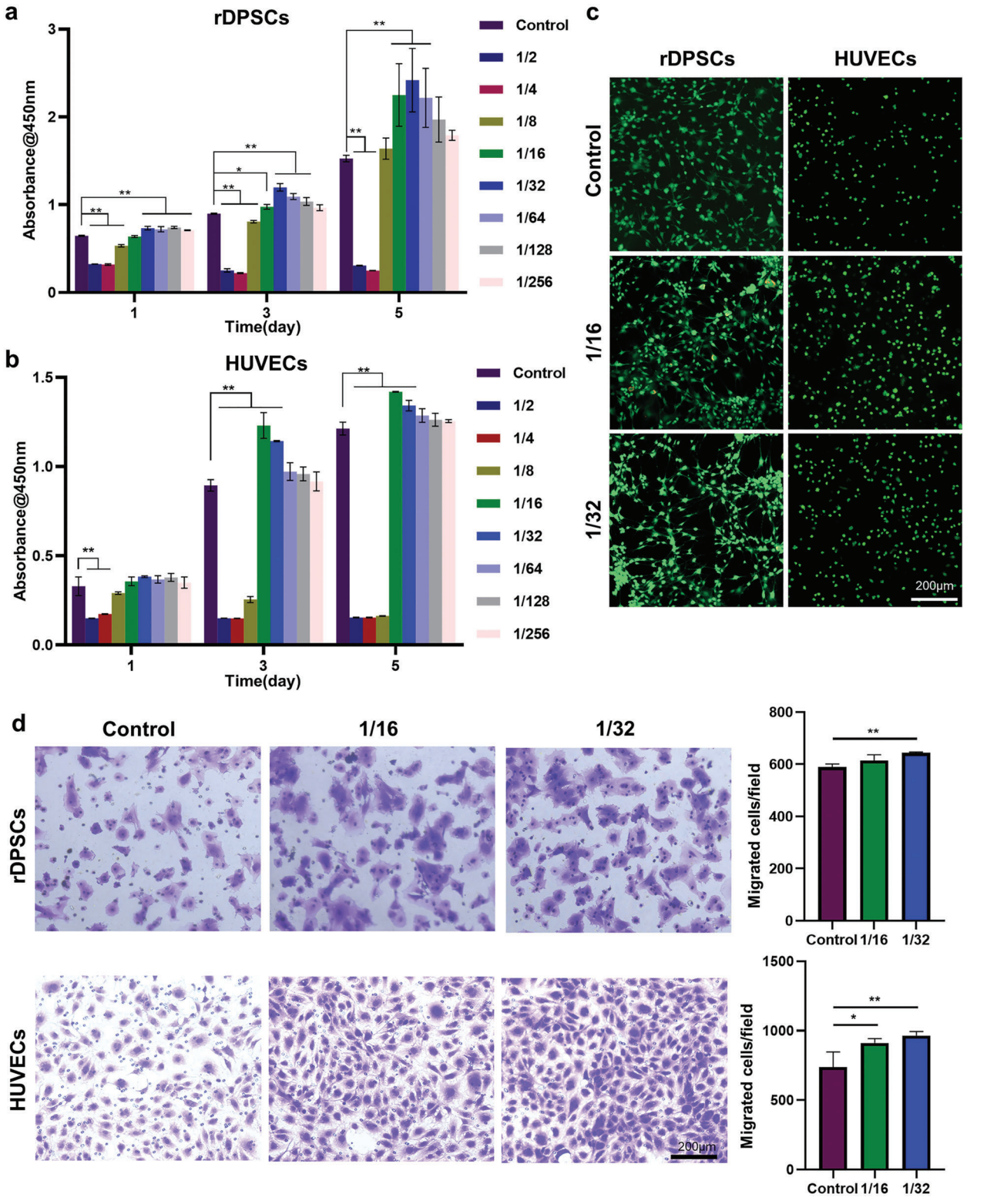

Figure 6. Effect of different concentrations of SC on the viability and migration of rDPSCs and HUVECs. a) CCK-8 assay results showing the enhanced proliferation of rDPSCs in the 1/16, 1/32, and 1/64 dilution groups. b) CCK-8 assay results showing the enhanced proliferation of HUVECs in the 1/16 and 1/32 dilution groups. c) Live (green)/dead (red) cell staining results confirming the biocompatibility of SC with 1/16 and 1/32 dilution ratios. d) Transwell assay results indicating increased HUVEC migration in the 1/16 and 1/32 dilution groups. Significantly increased rDPSC migration was observed only in the 1/32 dilution group but not in the 1/16 dilution group. The data are expressed as the means ± SDs ($n = 3$), p-values were calculated by one-way ANOVA with Dunnett's multiple comparison: not significant, $p > 0.05$; $^{*}p < 0.05$; $^{**}p < 0.01$.

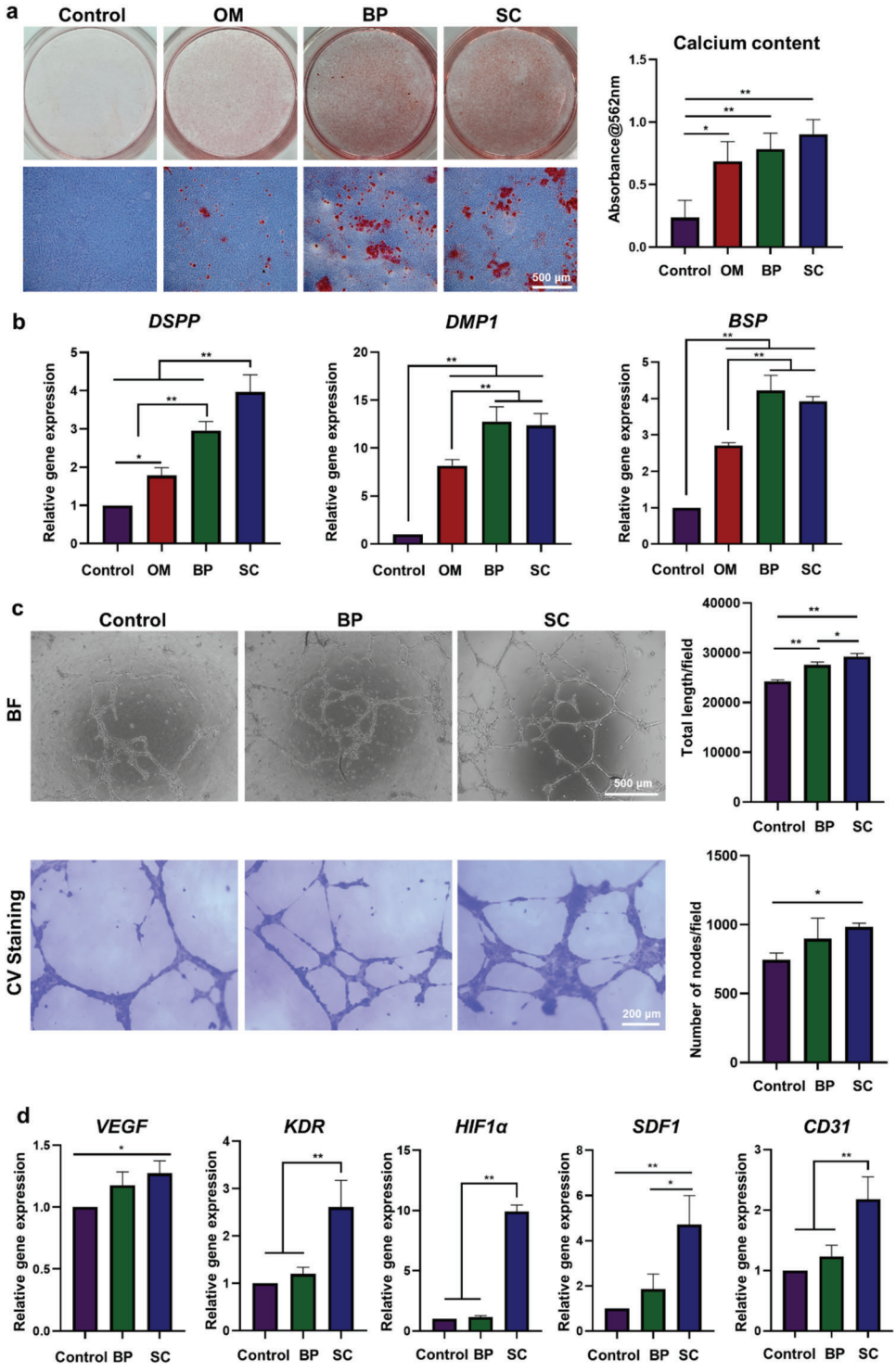

Figure 7. Effect of SC extract on the odontogenesis of rDPSCs and angiogenesis of HUVECs. a) Alizarin Red S staining and calcium deposit quantitative analysis results showing promoted mineralization in the OM group and significantly enhanced mineralization in the SC and BP groups compared to that in the OM group. b) Upregulation of odontogenic genes (*DSPP*, *DMP1*, and *BSP*) was detected in the SC and BP groups compared to that in the OM group. c) Images after culturing for 8 h showing enhanced tubule formation in the SC and BP groups. The quantification of the total length and number of nodes suggesting significantly increased tubular formation in the SC group compared to that in the BP and control groups. d) The upregulation of angiogenic genes (*VEGF*, *KDR*, *CD31*, *SDF1*, and *HIF1α*) was revealed in the SC group compared to that in the BP and OM groups. The data are expressed as the means ± SDs ($n = 3$), *p*-values were calculated by one-way ANOVA with Tukey's multiple comparison: not significant, $p > 0.05$; $^{*}p < 0.05$; $^{**}p < 0.01$.

large necrotic layer between the hydrogel and the remaining vital pulp. Sequentially, the collagen in this necrotic layer calcified and the stimulated rDPSCs odontogenic differentiated due to the excellent bioactivity of the $SrCuSi_4O_{10}$/GelMA hydrogel, leading to thick tertiary dentine formation and the higher expression of DSPP.[41]

Vascularization contributes to the formation of vessel-rich dental pulp and the recruitment of mesenchymal stem cells and provides nutritional support for cell differentiation and dentine bridge formation.[42] Cu, Sr, and Si have been proven to promote blood vessel formation and the expression of angiogenic genes, such as *HIF1α*, *VEGF*, and *KDR*.[19a,c,43] HIF1α has been demonstrated to induce hypoxia and stimulate VEGF expression.[44] Previous studies have suggested that VEGF and its receptor KDR are critical to the initiation process of vascularization.[45] SDF1 and CD31 are common markers indicating endothelial cell migration and cell–cell adhesion.[46] In angiogenesis assays of HUVECs, the SC group showed better angiogenic gene expression and tubular formation than the control and BP groups. The in vivo experiment results indicated that the SC/Gel+NIR group also exhibited increased vessel formation and CD31 expression. All of the above results suggested the capacity of $SrCuSi^4O_{10}$ to develop vascularization and odontogenesis, similar to the proven ability of $SrCuSi_4O_{10}$ to promote vascularized bone regeneration.[21]

All these results demonstrated that the $SrCuSi_4O_{10}$/GelMA composite hydrogel combined with NIR irradiation can be used as an effective strategy for the direct pulp capping of infected dental pulp due to the capability of this combined treatment to kill bacteria, inhibit biofilm growth and develop odontogenesis and angiogenesis. This study provides an innovative method for promoting dentine-pulp complex repair in infected dental pulp. However, this research is limited in terms of the biological function of $SrCuSi_4O_{10}$. Therefore, additional research on the mechanism of $SrCuSi_4O_{10}$-induced cell differentiation is needed. Moreover, NIR irradiation may be applicable for the induction of bone regeneration;[47] thus, the effect of 808 nm NIR irradiation on odontogenesis also needs to be studied in the future. In addition, the repair process of dental pulp tissues in humans is much slower than that in rats. Therefore, further studies are needed to test this material in randomized clinical trials.

4. Conclusion

We prepared a $SrCuSi_4O_{10}$/GelMA photothermal composite hydrogel and exploited it as a pulp-capping material for VPT. The as-prepared $SrCuSi_4O_{10}$/GelMA hydrogel had ion-release capability and NIR-induced photothermal properties. We demonstrated that the $SrCuSi_4O_{10}$/GelMA hydrogel combined with NIR irradiation eliminated *S. mutans* and *L. casei*, inhibited biofilm formation in vitro, and promoted dentine-pulp complex repair in a rat dental pulp infection model. Furthermore, we confirmed that the odontogenesis of rDPSCs and angiogenesis of HUVECs were enhanced by $SrCuSi_4O_{10}$.

5. Experimental Section

Materials: Strontium chloride hexahydrate ($SrCl_2{\cdot}6H_2O$), sodium metasilicate nonahydrate ($Na_2SiO_3{\cdot}9H_2O$), copper oxide (CuO), and ammonia hydroxide ($NH_3{\cdot}H_2O$) were purchased from Aladdin Reagent Co., Ltd. (Shanghai, China). GelMA was purchased from Cure Gel Co., Ltd. (Zhejiang, China). 2-Hydroxy-4'-(2-hydroxyethoxy)-2-methylpropiophenone (Irgacure 2959) was purchased from Sigma–Aldrich Trading Co., Ltd. (Shanghai, China).

Synthesis of $SrCuSi_4O_{10}$ Microparticles: $SrCuSi_4O_{10}$ microparticles were prepared using a hydrothermal method.[48] Briefly, $SrCl_2{\cdot}6H_2O$ solution (0.5 M, 5 mL), $Na_2SiO_3{\cdot}9H_2O$ solution (0.5 M, 20 mL), and CuO powder (0.2 g) were mixed together for 10 min. Then, the pH value of the mixture was first adjusted to 7 using an aqueous HCl solution (1 M) and then adjusted to 11 with ammonia hydroxide. Sequentially, the obtained mixture was transferred to a para-polyphenol-lined autoclave and heated at 250 °C for 48 h. Finally, the synthesized blue powder was washed with Milli-Q water and lyophilized for further use.

Preparation of Ion Extracts Derived from $SrCuSi_4O_{10}$ Microparticles: Briefly, the ion extracts derived from SC microparticles were prepared by soaking the microparticles in a serum-free medium with a weight-to-volume ratio of 1 g 5 mL^{-1} at 37 °C for 24 h. Then, the suspension was centrifuged at 6000 rpm for 20 min to remove the powders, and the supernatant was sterilized with a 0.22 μm Millipore filter. The extracts derived from BP were prepared using the similar method. For cell experiments, the obtained SC extracts were diluted to different ratios (1/2, 1/4, 1/8, 1/16, 1/32, 1/64, 1/128, and 1/256) with the serum-free medium.

Preparation of the $SrCuSi_4O_{10}$/GelMA Composite Hydrogel: First, GelMA solution containing photoinitiator was prepared by dissolving 1 g GelMA and 0.05 g Irgacure 2959 in 10 mL deionized water at 40 °C away from light. Then, SC/Gel composite hydrogels were prepared by mixing SC microparticles with different weight concentrations (0.5%, 1%, and 2%) in the GelMA solution, and a 365 nm UV light was applied to cure the hydrogel for 5 min. The obtained composite hydrogels were designated 0.5-SC/Gel, 1-SC/Gel, and 2-SC/Gel, respectively. Pure GelMA hydrogel was prepared following the same procedure.

Characterization of the $SrCuSi_4O_{10}$ Microparticles and $SrCuSi_4O_{10}$/GelMA Composite Hydrogels: The surface morphologies of the SC microparticles and the composite hydrogels were observed using a scanning electron microscope (SEM, SU8010, HITACHI, Japan). The elemental analysis of the SC microparticles was performed through energy-dispersive X-ray spectroscopy (EDS). The X-ray diffraction (XRD) patterns of the SC microparticles were collected with an X-ray diffractometer (D8 ADVANCE, Bruker, Germany). The absorption spectra of the SC microparticles were measured with a Fourier transform infrared spectrometer (FTIR, Tensor II, Bruker, Germany). The UV absorption spectra of the SC microparticles were measured using an UV–vis-NIR spectrometer (CARY5000, Agilent, USA). The ion concentrations of the extracts and the ions released from the composite hydrogels were assessed via an inductively coupled plasma mass spectrometer (ICP–MS, Agilent 7850, USA).

To assess the photothermal ability of the SC/Gel composite hydrogels, different concentrations of the composite hydrogels were irradiated with an 808 nm laser (1 W cm^{-2}) for 5 min, and the real-time temperature was recorded using an infrared thermal imaging instrument (FLIR, SC300, Arlington). Additionally, the temperature changes of the composite hydrogel (0.5-SC/Gel) under irradiation with different laser powers (1, 1.5, and 2 W cm^{-2}) for 5 min or heated by 5 repeated intervals of laser irradiation (heating for 5 min and then cooling to room temperature) were recorded with an infrared thermal imager.

Bacterial Culture: *S. mutans* (UA159) and *L. casei* (ATCC393) were used for the following experiments. *S. mutans* was cultured with brain-heart infusion (BHI, HuanKai Microbial, China) broth, and *L. casei* was cultured in de Man, Rogosa and Sharpe (MRS, HuanKai Microbial, China) broth. Bacteria were harvested at the exponential growth phase for experiments in this study.

In Vitro Antibacterial Assay: Hydrogel samples of the GelMA hydrogel and SC/Gel hydrogel were added to 24-well culture plates and crosslinked by exposure to 365 nm ultraviolet light, and iRoot® BP Plus (BP, Innovative BioCeramix, Canada) was added as a control material. Bacteria were centrifuged at 5000 rpm for 5 min, resuspended in phosphate-buffered saline (PBS, Gibco, USA), and diluted to a concentration of 1×10^8

CFU mL^{-1}. Subsequently, 10 µL of bacterial solution was added onto the hydrogel, and some of the hydrogel samples were heated to 50 °C under NIR laser irradiation (808 nm, 1.5 W cm^{-2}) for 15 min. The bacterial suspension without any treatment was used as the control group. After that, the bacterial suspension was resuspended in 1 mL of PBS. To directly observe the antibacterial effect, 100 µL of the bacterial suspension was spread on an agar plate, and photos were taken after culturing for 24 h. To calculate the survival rates of bacteria, the bacterial suspension was diluted 1, 10, and 100 times, 100 µL of the diluted solution was spread on an agar plate and left to culture for 24 h, and then the number of colonies was counted.

In Vitro Bacterial Growth Assay: GelMA hydrogel, SC/Gel hydrogel or BP samples were added to 250 µL of bacterial suspension (1×10^8 CFU mL^{-1}) cultured in 48-well plates. Some hydrogel samples were treated by NIR laser irradiation (808 nm, 1.5 W cm^{-2}) for 15 min. After culturing for 24 h, 100 µL bacterial suspension of each well was transferred into a 96-well plate, and the optical density (OD) values at 600 nm were measured. In addition, the bacterial suspension in each well was diluted 1000 times, and 5 µL of the diluted solution was inoculated onto agar plates. Images of bacterial colonies were captured after culturing for another 24 h.

In Vitro Biofilm Formation Inhibition Assay: Bacterial suspensions containing *S. mutans* and *L. casei* (1×10^8 CFU mL^{-1}) were cultured in BHI broth containing 0.2% sucrose, with the addition of the GelMA hydrogel, SC/Gel hydrogel or BP samples. After incubation in the dark or treatment with 808 nm NIR laser (1.5 W cm^{-2}, 15 min), bacteria were cultured at 37 °C for 24 h to form biofilms. The biofilms were stained with 0.1% crystal violet after being rinsed with PBS, and images were captured. For quantitative analysis of biomass, the OD values at 575 nm of the dye and acetic acid solution eluteswere measured. Moreover, the biofilms were also stained by carboxyfluorescein diacetate succinimidyl ester (CFSE, Thermo Fisher, USA) for live bacteria and propidium iodide (PI, Beyotime, China) for dead bacteria to measure the viability of the remaining bacteria. Subsequently, the stained biofilms were observed and imaged by a laser-scanning confocal microscope (Zeiss LSM 780, Zeiss, Germany) using excitation(Ex) at 492 nm and emission(Em) at 517nm for CFSE and Ex/Em = 535/617 nm for PI.

In Vivo Infected Dental Pulp Repair Assay: The sample size was calculated using PASS software to minimize the number of sacrificed animals. Assuming an alpha of 0.05, an effect size of 0.1753 and a power of 80%, at least 4 teeth were needed in each group. Considering the possibility of sample loss, 6 teeth were included per group. A total of 12 healthy male SD rats (aged 8 weeks, 300–350 g) were used after approval by the Institutional Animal Care and Use Committee, Sun Yat-Sen University (license number: SYSU-IACUC-2021-000922). Twenty-four upper first molar teeth (each group $n = 6$) were used to establish the bacteria-induced dental pulp infection model. The experimental approach was modified from a previously reported method.[29] Instead of *E. faecalis* as in the previous method, *S. mutans* and *L. casei* were selected for the induction of pulp infection in this study.[50] The rats were anesthetized using intraperitoneal injection of 1% sodium pentobarbital. The teeth were drilled with a diamond bur (FG1/2) under water cooling to create a round defect to expose the pulp chamber. Then, the hole was expanded to the size of a #50 K-file (SybronEndo, USA) followed by irrigation with 3% NaClO, 17% EDTA, and PBS. The teeth were divided into four groups: i) blank, ii) control, iii) SC/Gel, and iv) SC/Gel+NIR. Sterile PBS solution was added to the pulp tissue in the blank group. The pulp tissue of the control, SC/Gel and SC/Gel+NIR groups was added by *S. mutans* and *L. casei* (1×10^5 CFU 5 μL^{-1}), the SC/Gel hydrogel was then added to the SC/Gel group, and the SC/Gel hydrogel together with NIR laser irradiation (808 nm, 1.5 W cm^{-2}) was applied for the SC/Gel+NIR group. Subsequently, the pulp chambers were sealed with BP, and the teeth cavities were filled with a light-cured dental composite resin with dental adhesive. Six weeks after the operation, the animals were sacrificed, and their maxillary bones were collected. All the filling materials were examined carefully to ensure that there was no restoration failure.

Microcomputed Tomography (Micro-CT), Histological Analysis, and Immunohistochemical Analysis: After fixation with 4% paraformaldehyde (Servicebio, Wuhan, China), the maxillary bones were scanned using micro-CT (µCT-50, SCANCO Medical AG) with X-ray at 70 kV and 114 µA (resolution 10 µm). Next, the harvested teeth were decalcified with 10% EDTA for 8 weeks, dehydrated, embedded in paraffin and serially cut into 5 µm sections. The sections were stained with hematoxylin and eosin (H&E) for histological analysis. Histological sections were blindly evaluated by two experienced oral biologists. Pulp inflammation and mineralization were evaluated according to criteria and a grading system that were reported previously (**Table 2**).[49] The thicknesses of tertiary dentine were measured using ImageScope software. For immunohistochemical staining, the sections were permeabilized in 0.2% Triton X-100 for 10 min and then blocked with serum-based blocking buffer for 1 h. The samples were incubated with primary antibodies against DSPP (Santa Cruz Biotechnology, USA) or CD31 (Affinity Biosciences, China) overnight at 4 °C and with secondary fluorescent antibodies for 1 h at room temperature. After mounting with FluoroShield mounting medium with 4',6-diamidino-2-phenylindole (DAPI) (Abcam, Cambridge, UK), the slides were imaged with a laser-scanning confocal microscope (Zeiss LSM 780, Zeiss, Germany).

Isolation and Culture of Cells: As described previously, rDPSCs were isolated from dental pulp extracted from the rat upper incisor.[50] The cells were cultured in α-minimum essential medium (α-MEM, Gibco, USA) supplemented with 20% fetal bovine serum (FBS, Gibco, USA), 1% penicillin/streptomycin (Invitrogen, USA) and 1% GlutaMAX (Gibco, USA). At 80% confluence, the rDPSCs were trypsinized and passaged, followed by culture in normal culture medium containing α-MEM, 10% FBS, 1% penicillin/streptomycin and 1% GlutaMAX. HUVECs were purchased from Zhong Qiao Xin Zhou Biotechnology Co., Ltd. (Shanghai, China) and were cultured in endothelial cell medium (ECM, ScienCell, USA) supplemented with 5% FBS (ScienCell, USA), 1% penicillin/streptomycin (ScienCell, USA) and 1% endothelial cell growth supplement (ScienCell, USA). All cells were cultured at 37 °C with 5% CO_2. rDPSCs at passages 3–5 and HUVECs at passages 4–8 were used in the following experiments.

Cell Proliferation Assay: For cell proliferation analysis, HUVECs (2×10^3 cells per well) and rDPSCs (3×10^3 cells per well) were seeded in 96-well plates in the presence of SC microparticle extracts at various dilutions (1/2, 1/4, 1/8, 1/16, 1/32, 1/64, 1/128, and 1/256). After 1, 3, and 5 days of culturing, 10 µL of Cell Counting Kit (CCK)-8 reagent was added to each well in the 96-well plate, followed by incubation at 37 °C for 2 h. The OD values at 450 nm were measured using an enzyme-linked immunosorbent assay plate reader (Biotek Epoch2, USA).

Cell Viability Assay: The cell viability was determined by the live/dead assay. HUVECs (1×10^4 cells per well) and rDPSCs (2×10^4 cells per well) were separately seeded in 24-well plates, and the culture medium was replaced by 1/16 and 1/32 diluted SC microparticle extracts after 24 h. After incubation for 5 d, calcein-acetoxymethyl ester (AM) and PI dissolved in PBS were used to stain the live and dead cells. The cells were imaged with a confocal laser microscope (ZEISS Axio Observer, Germany).

Transwell Cell Migration Assay: Transwell assays were applied to investigate cell migration. HUVECs and rDPSCs (1.5×10^5 cells per well) suspended in 200 µL of serum-free culture medium were seeded onto Transwell inserts (pore size: 8 µm, Corning, USA) in 24-well plates with 1/16 and 1/32 diluted SC microparticle extracts. After incubation at 37 °C for 8 h, the cells remaining in the upper chambers were gently wiped with a cotton swab. Then, the polycarbonate membrane was washed with PBS, and the remaining cells were fixed with 4% paraformaldehyde for 15 min and stained with 0.1% crystal violet. The migrated cells were viewed with an optical microscope (ZEISS Axio Observer, Germany) and counted using ImageJ software.

In Vitro Mineralization Assay: rDPSCs were precultured on a 6-well culture plate with normal culture medium, SC microparticle extract or BP extract for 24 h. For inducing the osteogenic differentiation of rDPSCs, the culture medium was then changed to osteogenic medium (OM) containing 100 nM dexamethasone (Sigma–Aldrich, USA), 50 µM a-ascorbic acid (Sigma–Aldrich, USA), and 10 mM β-glycerophosphate (Sigma–Aldrich, USA). After 21 days of induction, rDPSCs were fixed with 4% paraformaldehyde for 30 min and stained with Alizarin Red (OriCell, Guangzhou, China)

Table 2. Evaluation criteria for rat pulp tissue response based on inflammation and mineralization.

Grade	Pulp inflammation	Pulp mineralization
0	No inflammation	No trace of mineralization in the pulp
1	Mild or slight inflammation	Increased deposition of hard tissue along the surface of the remaining pulp tissue
2	Moderate inflammation	Extensive deposition of hard tissue in the pulp
3	Severe inflammation and/or abscess formation	-

for 5 min. Mineralized nodules were observed and photographed. The mineralization was quantified by adding 10% cetylpyridinium chloride (Aladdin, Shanghai, China) to each well and measuring the OD values at 562 nm.

In Vitro Angiogenesis Assay: Matrigel (Corning, USA) was added to 48-well plates and incubated at 37 °C for 1 h for solidification, and then HUVECs (3×10^4 cells per well) cultured with SC microparticle extract, BP extract or normal culture medium were seeded on the Matrigel. At 6 h, optical images were taken with a microscope (ZEISS Axio Observer, Germany), and the total length and number of nodes were analyzed with ImageJ software. The cells stained with 0.1% crystal violet were observed under an optical microscope.

mRNA Expression: HUVECs and rDPSCs (2×10^4 cells per well) were precultured in 12-well plates with normal culture medium or the extract of SC microparticles or BP. The medium of rDPSCs was replaced by OM after 24 h. After 7 days of culture, total RNA was isolated and purified using an RNA-Quick Purification Kit (ESscience Biotech, Shanghai, China), and cDNA was synthesized using an all-in-one miRNA quantitative real-time polymerase chain reaction (qRT–PCR) detection kit (GeneCopoeia, Guangzhou, China) according to the manufacturer's instructions. RT–PCR was performed using Hieff UNICON qPCR SYBR Green Master Mix (YEASEN Biotech Co., Ltd, Shanghai, China), the housekeeping gene β-actin and specific primers (Tables S1 and S2, Supporting Information). RT–PCR was performed using the following protocol: 95 °C × 5', followed by 40–45 cycles at 95 °C × 10'', 60 °C × 20'', and 72 °C × 20''. Data from each group were obtained as the mean fold change of three independent samples.

Statistical Analysis: Every assay was performed at least in triplicate. The data were presented as means (in the photothermal-heating curves) and means ± standard deviations (SDs). The sample size for each experiment was indicated in the figure legends. The normal distribution of the data was tested using a normality test. One-way analysis of variance (ANOVA) followed by Tukey's post hoc test was applied to compare the mean of each group with the mean of every other group, and Dunnett's *t*-test was applied to compare the mean of each group with the mean of the control group. For the results of the histological evaluation, statistically significant differences were determined using Kruskal–Wallis H-test followed by Dunn's post hoc test. Values of $p < 0.05$ were determined to indicate statistical significance ($\alpha = 0.05$, $^{*}p < 0.05$, $^{**}p < 0.01$). The statistical analysis was performed using GraphPad Prism and SPSS software.

Supporting Information

Supporting Information is available from the Wiley Online Library or from the author.

Acknowledgements

This work was supported by the National Nature Science Foundation of China (nos. 81970925, 82201037, 32271386, and 82201041), Wenzhou Science and Technology Major Project (ZY2022028), seed grants from the Wenzhou Institute, University of Chinese Academy of Sciences (WIUCASQD2020013 and WIUCASQD2021030)

Conflict of Interest

The authors declare no conflict of interest.

Author Contributions

Y.Q. and J.T. contributed equally to this work. X.W., J.C., and C.Y. conceived and designed the project. Y.F. and L.S. synthesized and characterized new materials and performed physicochemical assays. Most experiments were performed by Y.Q., J.T., and S.K. with the help of Y.L., Y.C., and M.L. Y.Q. and J.T. wrote the manuscript with help from C.Y. All authors approved the final version of the manuscript.

Data Availability Statement

The data that support the findings of this study are available from the corresponding author upon reasonable request.

Keywords

angiogenesis, antibacterials, bioceramics, odontogenesis, photothermal therapy

Received: February 20, 2023
Revised: April 11, 2023
Published online: June 14, 2023

[1] a) F. E. Baldasso, C. P. Stürmer, S. B. Luisi, M. N. Petruzzi, R. K. Scarparo, J. A. De Figueiredo, *Microsc. Res. Tech.* **2012**, *75*, 1557; b) T. Larsen, N. E. Fiehn, *APMIS* **2017**, *125*, 376.
[2] a) P. M. H. Dummer, V. Franco, G. Gambarini, D. Orstavik, L. Tjaderhane, J. Whitworth, H. F. Duncan, K. M. Galler, P. L. Tomson, S. Simon, I. El-Karim, R. Kundzina, G. Krastl, T. Dammaschke, H. Fransson, M. Markvart, M. Zehnder, L. Bjorndal, *Int. Endod. J.* **2019**, *52*, 3; b) D. J. Caplan, J. W. Cai, G. S. Yin, B. A. White, *J. Public Health Dent.* **2005**, *65*, 90.
[3] H. F. Duncan, *Int. Endod. J.* **2022**, *55*, 497.
[4] D. Ricucci, J. F. Siqueira Jr., Y. Li, F. R. Tay, *J. Dent.* **2019**, *86*, 41.
[5] M. Zanini, M. Hennequin, P. Y. Cousson, *J. Endod.* **2016**, *42*, 1167.
[6] a) I. A. Mejare, S. Axelsson, T. Davidson, F. Frisk, M. Hakeberg, T. Kvist, A. Norlund, A. Petersson, I. Portenier, H. Sandberg, S. Tranaeus, G. Bergenholtz, *Int. Endod. J.* **2012**, *45*, 597; b) D. Ricucci, S. Loghin, J. F. Siqueira, *J. Endod.* **2014**, *40*, 1932.
[7] R. Cameron, E. Claudia, W. Ping, S. Erin, N. B. Ruparel, *J. Endod.* **2019**, *45*, 1119.
[8] a) V. M. Barbosa, A. Pitondo-Silva, M. Oliveira-Silva, A. S. Martorano, C. C. Rizzi-Maia, Y. T. C. Silva-Sousa, L. M. S. Castro-Raucci, W. R. Neto, *Braz. Dent. J.* **2020**, *31*, 611; b) I. Damlar, E. Ozcan, E. Yula, M. Yalcin, S. Celik, *Dent. Mater. J.* **2014**, *33*, 453.

[9] a) M. Godoy-Gallardo, U. Eckhard, L. M. Delgado, Y. J. D. D. Puente, M. Hoyos-Nogues, F. J. Gil, R. A. Perez, *Bioact. Mater.* **2021**, *6*, 4470; b) J. Li, X. M. Liu, Z. Zhou, L. Tan, X. B. Wang, Y. F. Zheng, Y. Han, D. F. Chen, K. W. K. Yeung, Z. D. Cui, X. J. Yang, Y. Q. Liang, Z. Y. Li, S. L. Zhu, S. L. Wu, *ACS Nano* **2019**, *13*, 11153.
[10] a) C. Y. Ning, X. L. Wang, L. H. Li, Y. Zhu, M. Li, P. Yu, L. Zhou, Z. N. Zhou, J. Q. Chen, G. X. Tan, Y. Zhang, Y. J. Wang, C. B. Mao, *Chem. Res. Toxicol.* **2015**, *28*, 1815; b) J. Milenkovic, J. Hrenovic, D. Matijasevic, M. Niksic, N. Rajic, *Environ. Sci.* **2017**, *24*, 20273.
[11] F. Heidenau, W. Mittelmeier, R. Detsch, M. Haenle, F. Stenzel, G. Ziegler, H. Gollwitzer, *J. Mater. Sci.-Mater. M* **2005**, *16*, 883.
[12] S. M. Sharker, S. M. Kim, S. H. Kim, I. In, H. Lee, S. Y. Park, *J. Mater. Chem. B* **2015**, *3*, 5833.
[13] S. H. Kim, E. B. Kang, C. J. Jeong, S. M. Sharker, I. In, S. Y. Park, *ACS Appl. Mater. Interfaces* **2015**, *7*, 15600.
[14] a) D. He, X. Zhang, X. Yao, Y. Yang, *Colloids Surf. B Biointerfaces* **2022**, *211*, 112318; b) H. Yan, H. Ni, J. Jia, C. Shan, T. Zhang, Y. Gong, X. Li, J. Cao, W. Wu, W. Liu, Y. Tang, *Anal. Chem.* **2019**, *91*, 5225.
[15] W. X. Lei, K. F. Ren, T. T. Chen, X. C. Chen, B. C. Li, H. Chang, J. Ji, *Adv. Mater. Interfaces* **2016**, *3*, 1600767.
[16] Q. Xu, M. L. Chang, Y. Zhang, E. D. Wang, M. Xing, L. Gao, Z. G. Huan, F. Guo, J. Chang, *ACS Appl. Mater. Interfaces* **2020**, *12*, 31255.
[17] a) W. W. Peng, Z. G. Huan, G. Pei, J. H. Li, Y. Cao, L. Jiang, Y. Q. Zhu, *Dent. Mater. J.* **2022**, *41*, 27; b) H. Y. Li, K. Xue, N. Kong, K. Liu, J. Chang, *Biomaterials* **2014**, *35*, 3803.
[18] C. Rombouts, T. Giraud, C. Jeanneau, I. About, *J. Dent. Res.* **2017**, *96*, 137.
[19] a) C. T. Wu, Y. H. Zhou, M. C. Xu, P. P. Han, L. Chen, J. Chang, Y. Xiao, *Biomaterials* **2013**, *34*, 422; b) M. Huang, R. G. Hill, S. C. F. Rawlinson, *Acta Biomater.* **2016**, *38*, 201; c) W. Lu, C. Zhou, Y. Ma, J. Li, J. M. Jiang, Y. Q. Chen, L. Q. Dong, F. M. He, *Biomater. Sci.-UK* **2022**, *10*, 2198.
[20] C. Yang, M. R. Younis, J. Zhang, J. L. Qu, J. Lin, P. Huang, *Small* **2020**, *16*, 2001518.
[21] C. Yang, H. S. Ma, Z. Y. Wang, M. R. Younis, C. Y. Liu, C. T. Wu, Y. X. Luo, P. Huang, *Adv. Sci.* **2021**, *8*, 2100894.
[22] K. Yue, G. Trujillo-de Santiago, M. M. Alvarez, A. Tamayol, N. Annabi, A. Khademhosseini, *Biomaterials* **2015**, *73*, 254.
[23] A. Ratep, I. Kashif, *J. Mater. Sci.-Mater. El* **2021**, *32*, 12340.
[24] a) C. Parvathiraja, S. Shailajha, *Appl. Nanosci.* **2021**, *11*, 1411; b) N. S. Hassan, A. A. Jalil, M. A. H. Satar, C. N. C. Hitam, F. F. A. Aziz, A. A. Fauzi, M. A. A. Aziz, H. Bahruji, *Top. Catal.* **2020**, *63*, 1005.
[25] F. El-Sayed, M. S. A. Hussien, T. H. AlAbdulaal, A. H. Abdel-Aty, H. Y. Zahran, I. S. Yahia, M. S. Abdel-wahab, E. H. Ibrahim, M. A. Ibrahim, H. Elhaes, *J. Mater. Res. Technol.* **2022**, *20*, 959.
[26] I. Garofano, A. Duran, J. L. Perez-Rodriguez, M. D. Robador, *Spectrosc. Lett.* **2011**, *44*, 560.
[27] L. M. Lin, D. Ricucci, T. M. Saoud, A. Sigurdsson, B. Kahler, *Aust. Endod. J.* **2020**, *46*, 154.
[28] a) K. F. Lovato, C. M. Sedgley, *J. Endodont.* **2011**, *37*, 1542; b) M. Parirokh, M. Torabinejad, *J. Endodont.* **2010**, *36*, 16.
[29] A. El-Fiqi, N. Mandakhbayar, S. B. Jo, J. C. Knowles, J. H. Lee, H. W. Kim, *Bioact. Mater.* **2021**, *6*, 123.
[30] a) C. C. Sun, Y. N. Xie, X. L. Hu, J. N. Fu, J. Zhou, L. G. Wu, *J. Endodont.* **2020**, *46*, 763; b) I. N. Rocas, F. R. F. Alves, C. T. C. C. Rachid, K. C. Lima, I. V. Assuncao, P. N. Gomes, J. F. Siqueira, *PLoS One* **2016**, *11*, e0154653; c) I. N. Rocas, K. C. Lima, I. V. Assuncao, P. N. Gomes, I. V. Bracks, J. E. Siqueira, *J. Endod.* **2015**, *41*, 1450.
[31] G. Sundqvist, D. Figdor, S. Persson, U. Sjögren, *Oral Surg. Oral Med. Oral Pathol. Oral Radiol. Endod.* **1998**, *85*, 86.
[32] a) J. L. Sanz, L. Forner, C. Llena, J. Guerrero-Girones, M. Melo, S. Rengo, G. Spagnuolo, F. J. Rodriguez-Lozano, *J. Clin. Med.* **2020**, *9*, 3872; b) S. Shi, Z. F. Bao, Y. Liu, D. D. Zhang, X. Chen, L. M. Jiang, M. Zhong, *Int. Endod. J.* **2016**, *49*, 154.
[33] a) M. C. Allwood, A. D. Russell, *J. Bacteriol.* **1968**, *95*, 345; b) A. D. Russell, *Sci. Prog.* **2003**, *86*, 115.
[34] Y. F. Liu, N. Nie, H. F. Tang, C. R. Zhang, K. Z. Chen, W. Wang, J. F. Liu, *ACS Appl. Mater. Interfaces* **2021**, *13*, 11631.
[35] a) M. Li, L. Q. Li, K. Su, X. M. Liu, T. J. Zhang, Y. Q. Liang, D. D. Jing, X. J. Yang, D. Zheng, Z. D. Cui, Z. Y. Li, S. L. Zhu, K. W. K. Yeung, Y. F. Zheng, X. B. Wang, S. L. Wu, *Adv. Sci.* **2019**, *6*, 1900599; b) M. Y. Mao, W. J. Zhang, Z. W. Huang, J. Huang, J. Wang, W. P. Li, S. S. Gu, *Int. J. Nanomed.* **2021**, *16*, 7727.
[36] a) M. Lin, F. Xu, T. J. Lu, B. F. Bai, *Dent. Mater.* **2010**, *26*, 501; b) C. D. Lynch, J. L. Roberts, A. Al-Shehri, P. J. Milward, A. J. Sloan, *J. Dent.* **2018**, *79*, 11.
[37] a) B. Kruppke, S. Ray, V. Alt, M. Rohnke, C. Kern, M. Kampschulte, C. Heinemann, M. Budak, J. Adam, N. Dohner, L. Franz-Forsthoffer, T. El Khassawna, C. Heiss, T. Hanke, U. Thormann, *Molecules* **2020**, *25*, 5103; b) A. Bakhit, N. Kawashima, K. Hashimoto, S. Noda, K. Nara, M. Kuramoto, K. Tazawa, T. Okiji, *Sci. Rep.* **2020**, 10, 8375.
[38] A. Almushayt, K. Narayanan, A. E. Zaki, A. George, *Gene Ther.* **2006**, *13*, 611.
[39] F. Decup, N. Six, B. Palmier, D. Buch, J. J. Lasfargues, E. Salih, M. Goldberg, *Clin. Oral Investig.* **2000**, *4*, 110.
[40] J. Q. Feng, X. Luan, J. Wallace, D. Jing, T. Ohshima, A. B. Kulkarni, R. N. D'Souza, C. A. Kozak, M. MacDougall, *J. Biol. Chem.* **1998**, *273*, 9457.
[41] U. Schroder, *J. Dent. Res.* **1985**, *64*, 541.
[42] a) K. Xia, Z. Chen, J. Chen, H. X. Xu, Y. F. Xu, T. Yang, Q. Zhang, *Int. J. Nanomed.* **2020**, *15*, 6631; b) Y. Sueyama, T. Kaneko, T. Ito, R. Kaneko, T. Okiji, *J. Endod.* **2017**, *43*, 943.
[43] a) F. Liu, X. Zhang, X. Yu, Y. Xu, T. Feng, D. Ren, *J. Mater. Sci. Mater. Med.* **2011**, *22*, 683; b) F. Ma, Y. Zhang, L. Hu, Y. Peng, Y. Deng, W. He, Y. Ge, B. Tang, *Int. J. Biol. Macromol.* **2021**, *181*, 452.
[44] P. Maxwell, K. Salnikow, *Cancer Biol. Ther.* **2004**, *3*, 29.
[45] N. Ferrara, *J. Mol. Med.* **1999**, *77*, 527.
[46] a) J. T. Miller, J. H. Bartley, H. J. C. Wimborne, A. L. Walker, D. C. Hess, W. D. Hill, J. E. Carroll, *BMC Neurosci.* **2005**, *6*, 63; b) H. M. DeLisser, M. Christofidou-Solomidou, R. M. Strieter, M. D. Burdick, C. S. Robinson, R. S. Wexler, J. S. Kerr, C. Garlanda, J. R. Merwin, J. A. Madri, S. M. Albelda, *Am J. Pathol.* **1997**, *151*, 671.
[47] R. Kunimatsu, H. Gunji, Y. Tsuka, Y. Yoshimi, T. Awada, K. Sumi, K. Nakajima, A. Kimura, T. Hiraki, T. Abe, H. Naoto, M. Yanoshita, K. Tanimoto, *Lasers Med. Sci.* **2018**, *33*, 959.
[48] Y. Chen, M. Y. Shang, X. F. Wu, S. H. Feng, *CrystEngComm* **2014**, *16*, 5418.
[49] S. H. Choi, J. H. Jang, J. T. Koh, H. S. Chang, Y. C. Hwang, I. N. Hwang, B. N. Lee, W. M. Oh, *J. Endod.* **2019**, *45*, 1332.
[50] J. Tian, W. Y. Chen, Y. H. Xiong, Q. E. Li, S. Y. Kong, M. J. Li, C. F. Pang, Y. Qiu, Z. Z. Xu, Q. M. Gong, X. Wei, *Bioact. Mater.* **2023**, *22*, 326.